Available online at www.sciencedirect.com
SCIENCE DIRECT
Applied Catalysis B: Environmental 66 (2006) 100–110
APPLIED CATALYSIS B ENVIRONMENTAL
www.elsevier.com/locate/apcatb

Photocatalytic properties of nanosized Bi_2WO_6 catalysts synthesized via a hydrothermal process

Hongbo Fu, Liwu Zhang, Wenqing Yao, Yongfa Zhu *

Department of Chemistry, Tsinghua University, Beijing 100084, PR China

Received 20 October 2005; received in revised form 16 February 2006; accepted 17 February 2006
Available online 18 April 2006

Abstract

Nanosized Bi_2WO_6 was synthesized by a hydrothermal crystallization process. The as-prepared samples were characterized by X-ray diffraction, Brunauer–Emmet–Teller surface area and porosity measurements, transmission electron microscopy, Raman spectra, and diffuse reflectance spectroscopy. The photoactivities of the as-prepared samples for the rhodamine-B photodegradation were investigated systematically. As a result, the sample prepared at 180 °C exhibited the highest photochemical activity under visible-light irradiation. The further experiments revealed that the catalyst was active in a wide spectral range. Density functional theory calculations suggested that the visible-light response was due to the transition from the valence band formed by the hybrid orbitals of Bi 6s and O 2p to the conduction band of W 5d. The photoactivity of the catalyst in relationship with the hydrothermal temperature, the crystal and band structure were also discussed in detail.

Keywords: Photocatalytic; Nanosized Bi_2WO_6; Hydrothermal synthesis; Rhodamine-B; Visible-light

1. Introduction

In the past decades, photocatalytic degradation of harmful pollutants by semiconductors has received considerable attention [1–5]. Outstanding stability and oxidative power make TiO_2 the best semiconductor photocatalyst for environmental remediation. Many persistent organic substances were degraded in TiO_2 suspensions. Even so, slow reaction rate and poor solar efficiency (maximum 5%) have hindered the commercialization of this technology [6–9]. Therefore, in an attempt to eliminate these drawbacks, many studies on modifying surface or bulk properties of TiO_2, including doping [10–12], codeposition of metals, surface chelation [13], and mixing of two semiconductors [14], have been performed.

On the other hand, many researchers have diverted their attention to exploit new photocatalyst. The outstanding work done by Zou et al. [15] displayed that water splitting for H_2 and O_2 evolution in a stoichiometric amount over $NiO_x/In_{0.9}Ni_{0.1}TaO_4$ photocatalyst under visible-light irradiation. Other mixed oxides, such as $SrTiO_3$ [16], $NaTaO_3$ [17], ZrO_2 [18], $K_4Nb_6O_{17}$ [19], Ta_2O_5 [20], $BaTi_4O_9$ [21], and $CaIn_2O_4$ [22], have been reported to show high activities. However, only a few studies have been made so far with the aim of environmental clean-up [22].

Nanostructured tungstate materials, such as $CdWO_4$, $ZnWO_4$, and $BaWO_4$, have aroused much interest because of their potential application in various fields, such as in photoluminescence, microwave applications, optical fibers, scintillator materials, and catalysis [23,24]. Due to their unique combination of physical and chemical properties, in terms of molecular and electronic versatility, reactivity, and stability, it is reasonable to believe they may be a promising class of photocatalysts. As expected, Kudo and Hijii [25] have demonstrated photocatalytic O_2 evolution over Bi_2WO_6 from $AgNO_3$ solution. More recently, Zou et al. [26] have reported that Bi_2WO_6 showed not only the activity for photocatalytic O_2 evolution from H_2O, but also the activity of mineralizing both $CHCl_3$ and CH_3CHO under visible-light irradiation. Therefore, the photocatalyst with a strong oxidizing potential could be postulated. However, up to date, we have the dearth of information about the photophysical and photochemical properties of this material. There is an urgent need to observe this photocatalyst systematically.

Recently, many studies have been reported on the preparation and characterization of various nanosized semiconductors. The

* Corresponding author. Tel.: +86 10 6278 3586; fax: +86 10 6278 7601.
E-mail address: zhuyf@mail.tsinghua.edu.cn (Y. Zhu).

0926-3373/$ – see front matter © 2006 Elsevier B.V. All rights reserved.
doi:10.1016/j.apcatb.2006.02.022

nanoparticles exhibit special photochemical characteristics [8]. In particular, the band gap of nanoparticles increases with the decrease of the size, resulting in a stronger photocatalytic power. Other important properties such as optical and physical absorption and luminescence emission also undergo drastic changes [24].

In a previous study [27], we have successfully synthesized Bi_2WO_6 nanoplates by a simple hydrothermal process, and a detailed growth mechanism of Bi_2WO_6 nanoplates was also clarified. In the present study, to further understand photocatalytic properties of nanostructured Bi_2WO_6 catalyst, Bi_2WO_6 catalysts were firstly prepared via the hydrothermal synthesis at different temperature. Bulk and surface characterizations of the powders were carried out by means of X-ray diffractometry (XRD), Brunauer–Emmet–Teller (BET) specific surface areas and porosity measurements, transmission electron microscopy (TEM), laser Raman spectra (LRS), and diffuse reflectance (DR) spectroscopy. The energy band dispersion diagram and density of state (DOS) were obtained by the plane-wave-density function theory (DFT) calculation. The photoactivities of the as-prepared samples for the rhodamine-B (RhB) photodegradation were systematically investigated. We expected to provide useful information for a greater understanding of the Bi_2WO_6 photocatalysis from the mechanistic and kinetic viewpoints.

2. Experimental

2.1. Catalyst preparation

Bi_2WO_6 was prepared via the hydrothermal synthesis according to the previous literature [24,27]. In a typical synthesis procedure, 0.485 g $Bi(NO_3)_3{\cdot}5H_2O$, 0.125 H_2WO_4 and 0.28 g KOH were added to 9 mL deionized water with magnetic stirring. A series of the reaction mixtures were sealed in a Teflon-lined stainless steel autoclave and heated in the temperature range 120–200° C under autogenous pressure for 24 h. After cooling, the product was filtered, washed and dried at ambient temperature. All chemicals were reagent grade quality and used without further purification. Deionized and doubly distilled water were used throughout this study. $TiO_{2-x}N_x$, known for its good photocatalytic activity in decomposition of the pollutants under visible-light irradiation, was also prepared as a reference [10].

2.2. Sample characterization

The particle sizes have been determined using a JEOL JEM-1200EX TEM. Specific surface areas were determined in a Flow Sorb 2300 apparatus (Micromeritics) using a single-point BET method. Porosity was monitored using a Sorptomatic 1900 Carlo Erba Instrument from the nitrogen adsorption-desorption isotherms obtained at −196° C. XRD patterns of the powders were recorded at room temperature with a Bruker D8 Advance XRD with Cu Kα radiation. UV–vis DR spectra were obtained using a Hitachi U-3010 spectroscopy. LRS were obtained using a Renishaw RM2000 spectrometer equipped with notch filter and a CCD detector. Total organic carbon (TOC) was measured with a Tekmar Dohrmann Apollo 9000 TOC analyzer. NH_4^+ and NO_3^- ions were analyzed with a Shimadzu LC-10AS ion chromatograph. The ratio of Bi/W in the sample was determined with a sequential X-ray fluorescence spectrometer (XRF-1700, Shimapzu).

2.3. Photochemical experiments

The photocatalytic activities of the samples were evaluated by the RhB decomposition under UV and visible-light irradiation. UV light was obtained by a 12 W Hg lamp (λ = 254 nm, the Institute of Electric Light Sources, Beijing) and the average light intensity was 50 μW cm^{-2}. In the case of visible-light irradiation, a 500 W xenon lamp ($\lambda > 290$ nm, the Institute of Electric Light Sources, Beijing) was focused through a window. A 420 or 490 nm cutoff filter was placed onto the window face of the cell to ensure the desired irradiation condition. The average light intensity was 40 or 30 mW cm^{-2}, respectively. The radiant flux was measured with a power meter (the Institute of Electric Light Sources, Beijing).

Aqueous suspensions (usually 100 mL) of RhB (1×10^{-5} M) and Bi_2WO_6 powder (0.5 g L^{-1}) were placed in a vessel. Prior to irradiation, the suspensions were magnetically stirred in the dark for ca. 30 min to ensure the adsorption/desorption equilibrium. At given time intervals, 3 mL aliquots were sampled, and centrifugated to remove the particles. The filtrates were analyzed by recording the variations of the absorption band maximum (553 nm) in the UV–vis spectrum of RhB using a Hitachi U-3010 spectrophotometer.

3. Results

3.1. Sample characterization

The morphologies and microstructures of the as-prepared samples were firstly investigated with TEM. The results are shown in Fig. 1. The morphologies and dimensions of the samples are strongly dependent on the hydrothermal temperature. Fig. 1A shows TEM micrograph of the sample prepared at 120° C, nanosized Bi_2WO_6 crystals display mainly thin sheet-shaped morphology and the border lengths of the thin sheets are a few hundreds of nanometer. As the hydrothermal temperature goes up to 140° C, the mixtures of sphere- and sheet-shaped crystals can be seen (Fig. 1B). The crystallite size is several dozens of nanometers. With the increase of the hydrothermal temperature to 160° C, the homogenous sphere-shaped morphologies can be seen. The sizes of these crystals are in the scope of 20–50 nm (Fig. 1C). For the higher-temperature reaction, such as 180 and 200° C, the sheet-shaped crystals are regained. The samples hold the large primary sheets and smaller secondary ones. The close-folded agglomerations of the irregular sheets are clearly seen (Fig. 1D and E).

The surface textural properties of the as-prepared samples were assessed by nitrogen adsorption measurements at −196° C. Fig. 2 shows nitrogen adsorption isotherms and pore size distributions. The curves are similar, irrespective of the

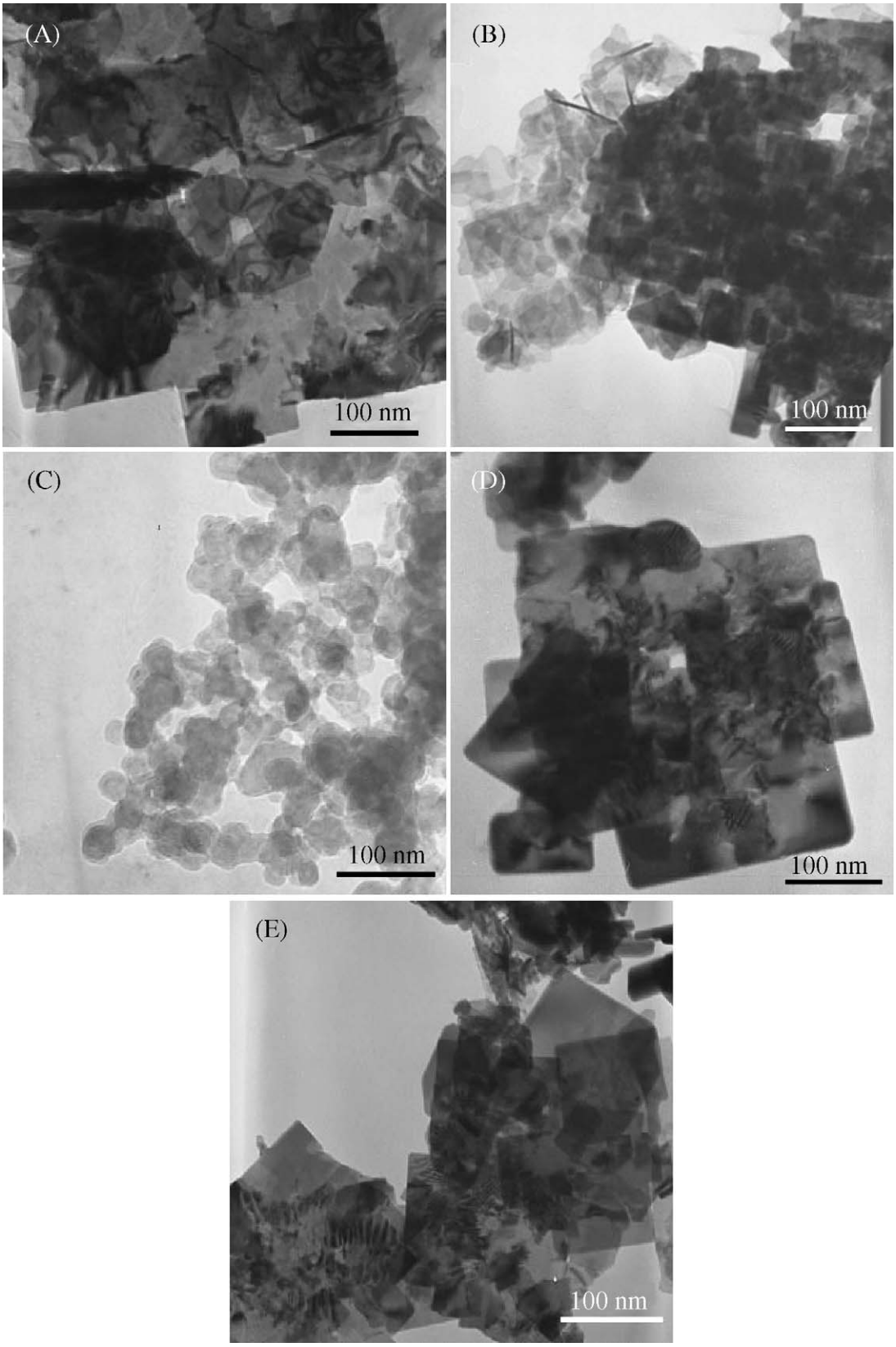

Fig. 1. TEM micrographs of the as-prepared samples: (A) 120 °C, (B) 140 °C, (C) 160 °C, (D) 180 °C, and (E) 200 °C.

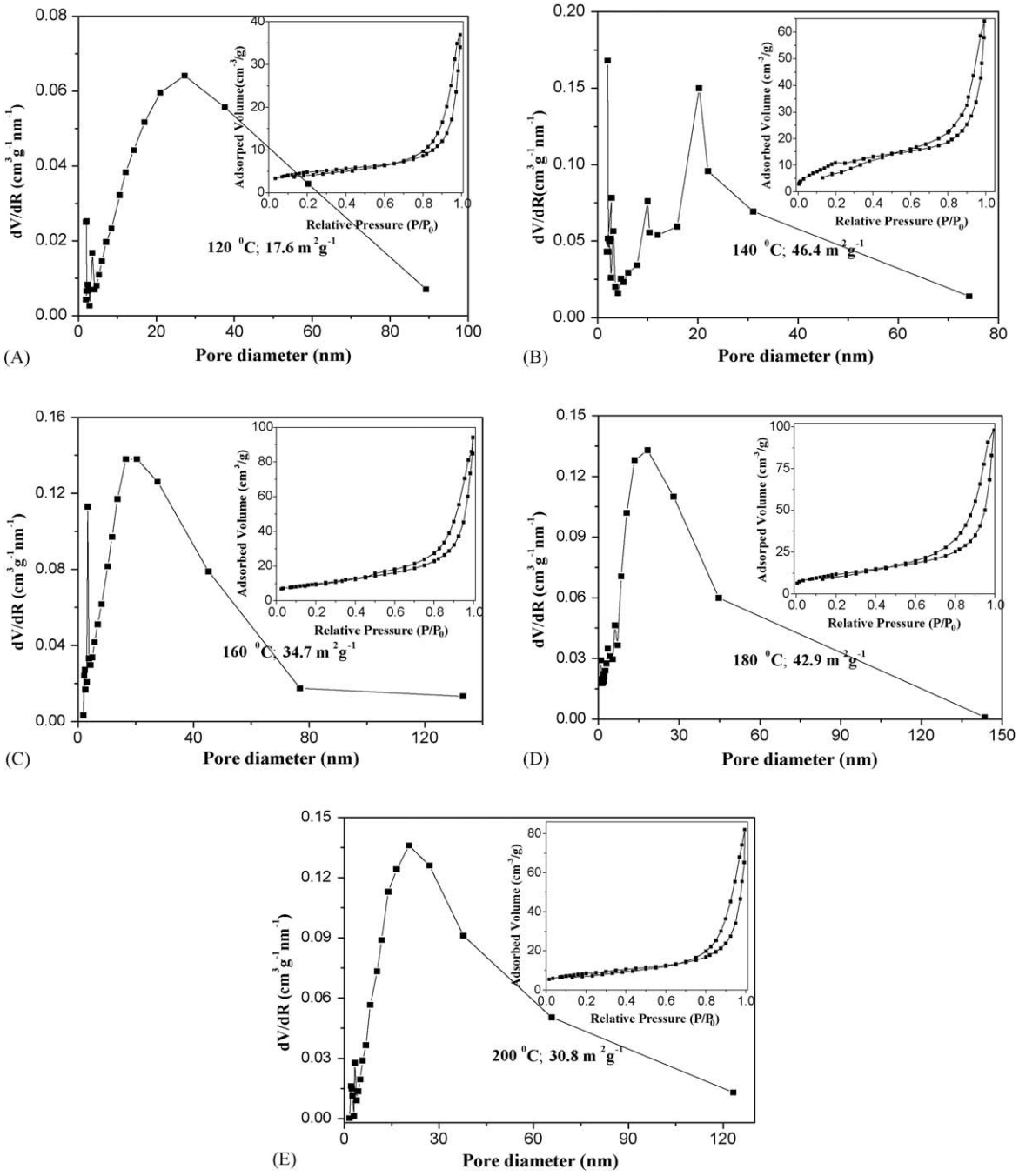

Fig. 2. N_2 adsorption-desorption isotherms (inset) and Barret–Joyner–Halenda (BJH) pore size distribution plots of the as-prepared samples.

hydrothermal temperature. The difference is the most significant for the sample prepared at 140° C. Clearly, two pore size distributions could be observed in Fig. 2B. A not so well defined pore size distribution is in agreement with the TEM result (Fig. 1B), which presented the mixtures of sphere- and sheet-shaped crystals. The pore size distribution of the sample prepared at 180° C is narrowest, suggesting that the crystals are the most monodisperse, compared to the other samples. The as-prepared samples exhibit the relatively high surface areas with respect to the one synthesized by the solid-state reaction method [17,26]. Even the sample was prepared at 120° C, its specific surface area is a rather high value of 17.6 $m^2\,g^{-1}$. The largest surface area of 46.4 $m^2\,g^{-1}$ is achieved when the sample is synthesized at 140° C. Except for this temperature, the sample prepared at 180° C also revealed the significant high surface area of 42.9 $m^2\,g^{-1}$. Specific surface area of the sample is not consequentially in association with the hydrothermal temperature.

To investigate the formation process of Bi_2WO_6 crystalloids, XRD patterns of the samples obtained at different temperature were measured, which are shown in Fig. 3. The temperature exerts a great influence on the formation of the crystals, as can be seen from the difference in the peaks at 28.3°, 33°, 47°, 55.8° and 58.5° in XRD patterns. It is clearly seen that the

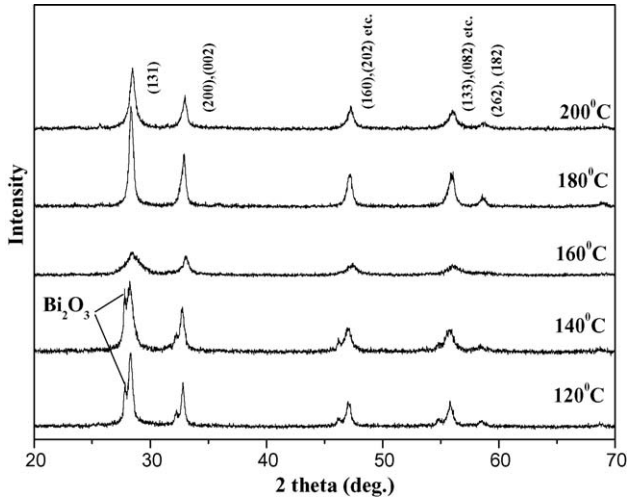

Fig. 3. XRD patterns of the as-prepared samples.

crystallization has occurred even at 120 °C. However, the notable impurity, such as Bi_2O_3, was detected below 140 °C. The sample finally becomes a homogeneous phase at 160 °C. When the temperature further goes up to 180 °C, the XRD pattern of the sample reveal the narrower peaks and the higher intensity, suggesting the enhanced crystallite size. For the sample prepared at 200 °C, the intensities of the diffraction peaks decrease a little, compared to the one prepared at 180 °C, suggesting the crystal phase become poorer. It was found that the standard intensity of the (1 1 3) peak is about five times than (2 0 0) or (0 2 0) peak which could be expressed as: $I_{(1\ 1\ 3)}/I_{(2\ 0\ 0)} = 5$. However, as for the sample prepared at 180 °C, the value of $I_{(1\ 1\ 3)}/I_{(2\ 0\ 0)}$ was almost smaller than 2, suggesting that the crystal has special anisotropic growth in (2 0 0) or (0 2 0) direction. These results could be attributed to their unique sheet-shaped morphologies. XRD results indicate that nanosized Bi_2WO_6 could be selectively synthesized by adjusting hydrothermal temperature, and well-crystallized Bi_2WO_6 crystals can be obtained at 180 °C.

LRS of the as-prepared samples are shown in Fig. 4. According to the report of Grane et al. [28], the peaks in the range 600–1000 cm^{-1} are assigned to the stretches of the W–O bands. In more detail, the bands at 790 and 820 cm^{-1} are associated with antisymmetric and symmetric A_g modes of terminal O–W–O. The band at 310 cm^{-1} can be assigned to translational modes involving simultaneous motions Bi^{3+} and WO_6^{6-}. The intensity of the peak at 700 cm^{-1} is interpreted as an antisymmetric bridging mode associated with the tungstate chain. As can be seen, a raise in temperature is connected with an increase in the intensities of the bands in the scope of 120–180 °C. The intensities of the peaks decrease as the hydrothermal temperature further rises from 180 to 200 °C, suggesting a reduction of crystallite size. High crystallinity could be achieved above 160 °C. These observations are in good agreement with TEM and XRD results. It is difficult to identify if there contain the impurity of Bi_2O_3, because the stretches of Bi_2O_3 are likely to overlap with ones of Bi_2WO_6 [28].

3.2. Photoabsorbance property and band structure

Fig. 5 shows DR spectra for the as-prepared samples. The samples present almost the same absorption edge around 440 nm. The sample prepared at 180 °C reveal the strongest absorbance in the region of 250–370 nm. Nevertheless, the considerable absorption of the catalyst in the visible-light region is expected to be responsible for the visible-light-induced photoactivity. The steep shapes of UV–vis DR spectra indicate that visible-light absorption is not due to the transition from the impurity level but is due to the band-gap transition [26]. For a crystalline semiconductor, the optical absorption near the band edge follows the equation below [16]:

$$ahv = A(hv - E_g)^n \quad (1)$$

where a, v, E_g, and A are absorption coefficient, light frequency, band gap, and a constant, respectively. The value of n decides the characteristics of the transition in a semiconductor. According to the equation, the value of n for Bi_2WO_6 was 1. The band

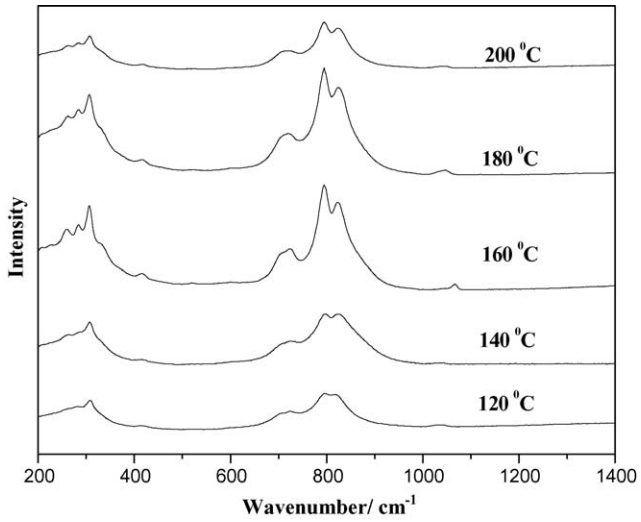

Fig. 4. LRS of the as-prepared samples.

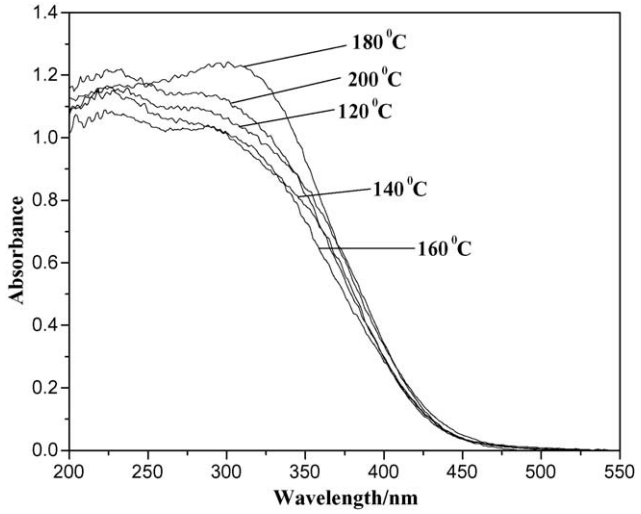

Fig. 5. UV–vis DR spectra of the as-prepared samples.

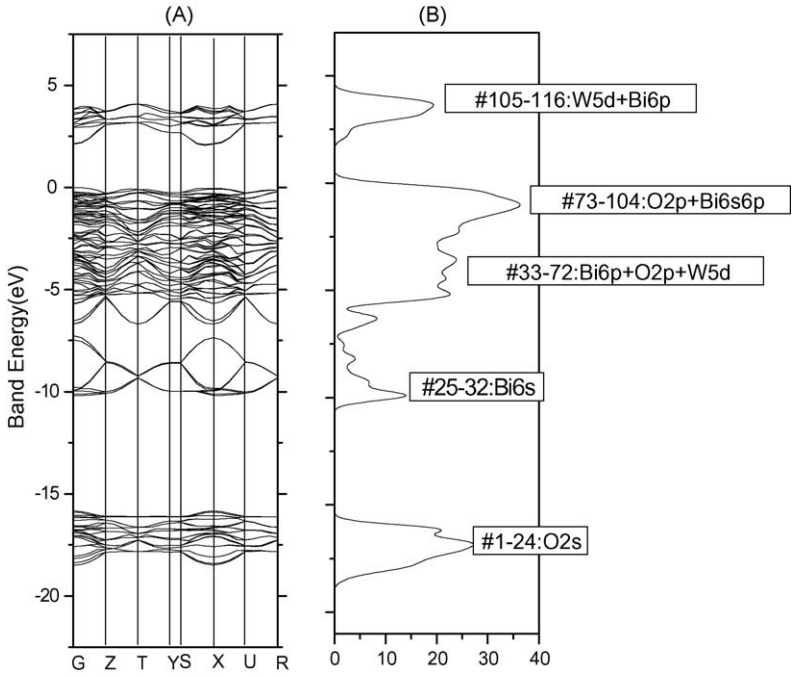

Fig. 6. Energy-band diagram (A) and density of states (B) for Bi_2WO_6 calculated by a DFT method.

gap of Bi_2WO_6 can be estimated as $E_g = 2.7$ eV. The colors of the photocatalysts are yellow, as can be expected from their absorption spectra.

The energy level and the band gap of the oxide semiconductor will play a crucial role in determining photocatalytic activity. On the basis of the crystal structure, the electronic structure of Bi_2WO_6 was first investigated by plane wave DFT calculations. Exchange-correlation effects were taken into account using the generalized gradient approximation (GGA) [29]. The total energy code CASTEP was used, which utilized pseudopotentials to describe electron–ion interactions and represented electronic wavefunctions using a plane-wave basis set [30]. The kinetic energy cutoff was set at 300 eV. The result is shown in Fig. 6.

The occupied bands of Bi_2WO_6 are classified into four bands. The lower-energy side in the occupied bands consists of solely O 2s orbitals (1–24#). The middle part of the occupied bands consist of Bi 6s orbitals (25–32#) and Bi 6p and O 2p and W 5d hybrid orbitals (33–72#), respectively. The higher-energy side, i.e., corresponding to a valence band (VB), consists of O 2p and Bi 6s hybrid orbitals, with a small contribution of Bi 6p orbitals (73–104#). The bottom of the conduction band (CB) is formed by the W 5d orbitals, and Bi 6p is included to some degree. Fig. 7 shows the density contour maps of orbitals with the highest occupied molecular orbital (HOMO) and the lowest unoccupied molecular orbital (LUMO). HOMO shows the p orbital of the O atom and the s and p orbitals of the Bi atom, indicating that the orbitals are composed of the O 2p and Bi 6s orbitals. LUMO is mainly formed by the W 5d orbital, but O 2p mix into to some degree. This mixing is rather common for metal oxide semiconductors including d^{10} elements [17,22]. Thus, the highest occupied and lowest unoccupied molecular orbital levels are composed of the hybrid orbitals of O 2p and Bi 6s and the W 5d orbitals, respectively. The band gap of Bi_2WO_6 was estimated to be 1.63 eV. Generally, the band gap calculated by DFT was smaller than that obtained experimentally, which is frequently pointed out as a common feature of DFT calculations [31]. The band structure indicates that the charge transfer upon photoexcitation occurs from the O 2p and Bi 6s hybrid orbitals to the empty W 5d orbitals. The band gap becomes narrower and the considerable absorption extends up to the visible region, which could be due to the transition from

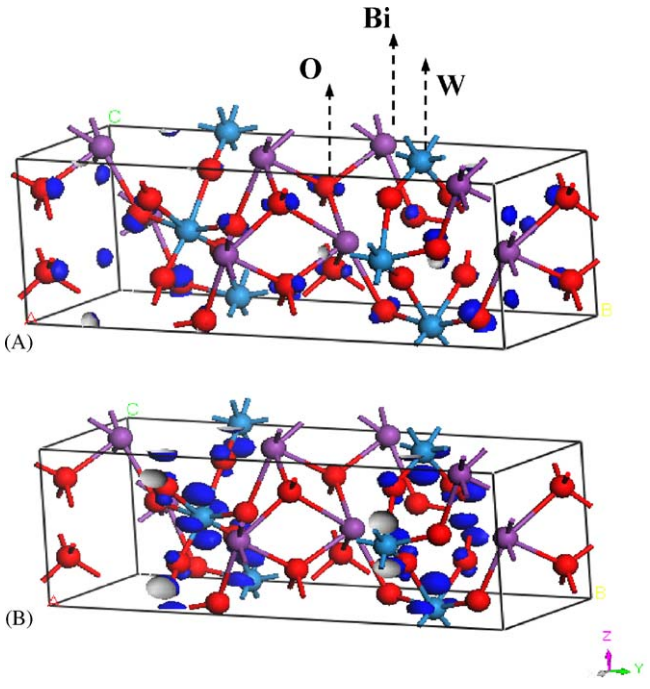

Fig. 7. Density contour maps for HOMOs (A) and LUMOs (B) of Bi_2WO_6.

the hybrid orbitals of Bi 6s and O 2p to the W 5d orbitals. Photooxidation of the pollutant over Bi_2WO_6 photocatalyst occurs as a result of contributions from the photoexcited holes in the VB consisting of the O 2p and Bi 6s hybrid orbitals.

3.3. Photocatalytic activity

On the basis of the surface characterization results described above, it is now instructive to compare the photocatalytic activities of all samples under visible-light ($\lambda > 420$ nm). The RhB photodegradation was tested as a model reaction to evaluate photocatalytic activities of the as-prepared samples. For comparison, the RhB photodegradation by $TiO_{2-x}N_x$ was also performed. The results are shown in Fig. 8. The RhB photodegradation over the catalysts is fitted for pseudo-first-order kinetics. The hydrothermal temperature has a significant effect on the degradation rate. The most samples exhibited the higher photoactivities than $TiO_{2-x}N_x$ under visible-light irradiation. Control experiments displayed that RhB did not degrade in Bi_2WO_6 suspension in the dark or when illuminated with visible-light at the absence of the catalyst. We inferred from this the catalyst and visible-light are indispensable to the RhB photodegradation. The determined reaction rate constant (k) was 0.091, 0.082, 0.061, 0.053, 0.032 and 0.023 min^{-1}, respectively, for the sample prepared at 180, 160, 200, 140 °C, $TiO_{2-x}N_x$ and 120 °C. In the range 120–180 °C, an increase in the hydrothermal temperature results in the acceleration of the RhB degradation. The sample prepared at 180 °C shows the highest photoactivity. However, the sample prepared at 200 °C reveals the lower activity to degrade RhB, compared to the sample prepared at 180 °C.

Bi_2WO_6 as a kind of heterogeneous photocatalyst can be easily recycled by a simple filtration. XRD analysis showed that crystal structure of the photocatalyst was not changed after the photocatalytic reaction, suggesting that Bi_2WO_6 catalyst is stable during the photocatalytic reaction. The stability of the photocatalyst may be related to the condition of hydrothermal synthesis. The hydrothermal method allows the crystallization of the catalyst under mild conditions over a long period of time. The catalyst crystallizing in hydrothermal condition indicates that it could show stable activity for the photodegradation of organic pollutants [32].

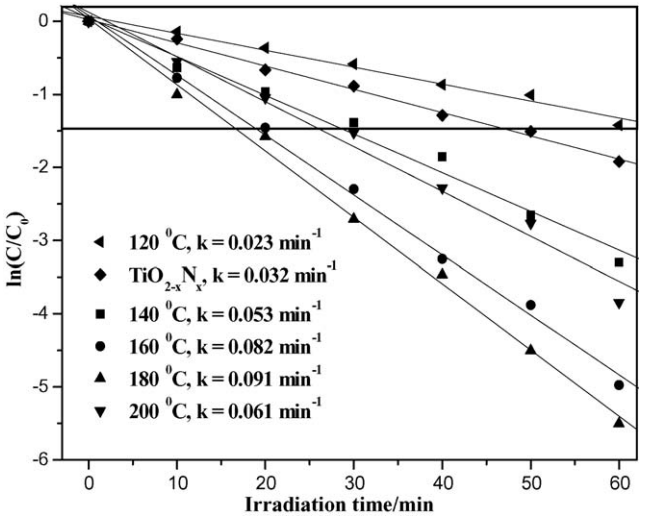

Fig. 8. Photocatalytic degradation of RhB over the as-prepared samples and $TiO_{2-x}N_x$ under visible-light irradiation ($\lambda > 420$ nm); catalyst loading, 0.5 g L^{-1}; RhB, 1×10^{-5} M.

To further understand the photochemical property of the catalyst, the RhB photodegradation by the sample prepared at 180 °C was performed under the different irradiation wavelength. The temporal evolution of the spectral changes taking place during the RhB photodegradation is shown in Fig. 9. RhB shows a major absorption band at 553 nm. In any case, irradiated by UV ($\lambda = 254$ nm) or visible-light ($\lambda > 420$ nm or $\lambda > 490$ nm), The aqueous RhB/Bi_2WO_6 suspension leads to an apparent decrease in absorption. Under UV irradiation, the absorbance of the suspension decreases dramatically. Absorption spectra reveal no evidence of the existence of new intermediates or products formed in the visible or near-ultraviolet region. The color of the suspension changes light gradually and disappear ultimately. However, under visible-light irradiation, the absorbance of the suspension decreases with a concomitant wavelength shift of the band to shorter wavelengths, and the new band around 500 nm occurs. The color of suspension changes from an initial red color to a final light green-yellow color.

The RhB decomposition, decrease of TOC, and formation of NH_4^+ in this photochemical process is also shown in Fig. 9. The photocatalyst showed very high photocatalytic activity both in the UV-light ($\lambda = 254$ nm) and visible-light ($\lambda > 420$ nm). Almost complete degradation of RhB was achieved when exposed to UV irradiation after 90 min. In the case of the light ($\lambda > 420$ nm), about 90% of RhB was degraded after 60 min. When the cutoff filter of 490 nm was employed, the photocatalyst was still active. Eighty-seven percent of RhB was transformed after 4 h. These results indicate that the catalyst is active in a wide spectral region. Clearly, TOC reduction was slower than the loss of RhB, suggesting that the intermediates occurred during the photochemical process. When 90% of RhB were transformed, about 67%, 41% and 43% of mineralized degree were reached in the case of UV irradiation ($\lambda = 254$ nm), visible irradiation ($\lambda > 420$ nm) and ($\lambda > 490$ nm), respectively. The higher mineralized degree could be achieved in the case of UV irradiation. In any case, NH_4^+ was easily inspected. However, NO_3^- formation from the photooxidative step was insignificant (<0.1 mg L^{-1}). This indicates that NH_4^+ is the main product of nitrogen transformation for the RhB photodegradation under the present conditions. It is notable that the yield of NH_4^+ in the case of UV irradiation is lower compared to that in the case of visible irradiation ($\lambda > 420$ nm or $\lambda > 490$ nm).

As a novel catalyst, UV-light induced activity of Bi_2WO_6 is not still reported. It is meaningful to compare its activity with P25 (TiO_2), which is well known a standard photocatalyst (see supporting information). The sample prepared at 180 °C was found not to be so active for the degradation of RhB compared to P25. This could be due to the poor dispersion of the catalyst in the solution. It was found that Bi_2WO_6 powder was accumulated at

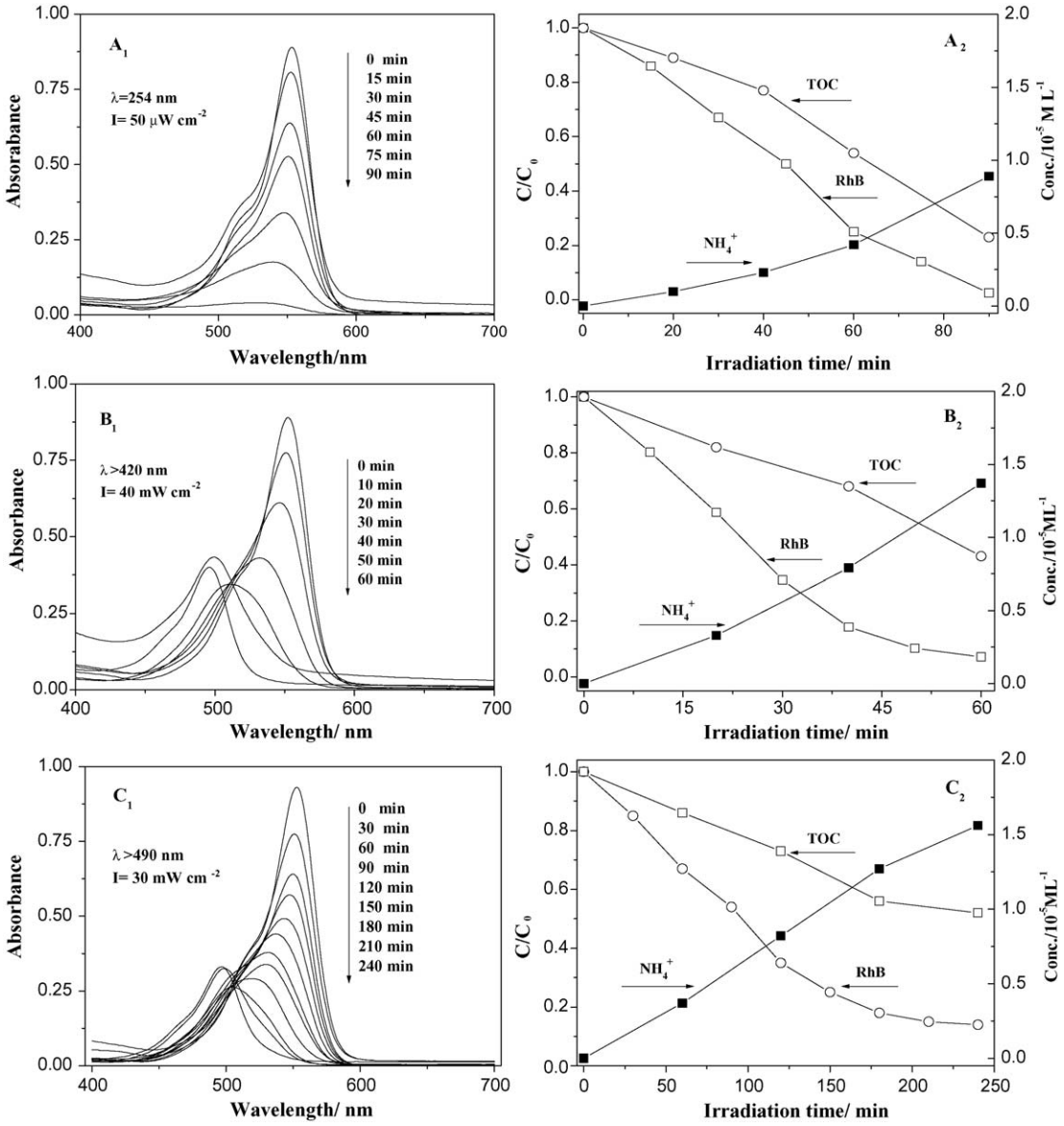

Fig. 9. UV–vis spectral changes of RhB in aqueous Bi_2WO_6 (prepared at 180 °C) suspensions under different irradiation wavelengths (A_1, B_1 and C_1), changes in the RhB concentration and formation of NH_4^+ (A_2, B_2 and C_2); catalyst loading, 0.5 g L^{-1}; RhB, 1×10^{-5} M.

the bottom of the reaction vessel during the course of the photochemical reaction due to its high density of 9.51 g cm^{-3} and unique sheet-shaped morphology. However, in the case of P25, the catalyst powder was suspended equably in the solution for a long time even after the experiment was finished. Undoubtedly, a heavily aggregated state of Bi_2WO_6 limits its activity greatly. The approach to improve the dispersion of the catalyst is under investigation and is expected to increase significantly the photocatalytic activity of this material.

4. Discussion

4.1. Hydrothermal temperature

The most important characteristic of Bi_2WO_6 samples prepared by the hydrothermal crystallization process is their relatively large surface areas. Indeed, the specific surface areas of the as-prepared samples are in the range 17.6–46.4 m^2 g^{-1}, while those prepared by solid-state reaction method are quite low, typically less than 1 m^2 g^{-1} [25]. It can be anticipated that our material with high surface areas exhibit the enhanced photoactivity, since the surface area of the photocatalyst affects the number of active sites in a photocatalytic reaction. The photodegradation rate of RhB over Bi_2WO_6 was plotted as a function of the reaction temperature in Fig. 10, wherein the data for the BET specific surface area of each sample were also included. The sample prepared at a lower temperature of 140 °C show the rate of only 0.053 min^{-1}, which is much less than that expected from their relatively large specific surface area of 46.4 m^2 g^{-1}. However, high photocatalytic activity is presented by the sample prepared at 180 °C. Obviously, high activity of the sample is related to its extremely high crystallinity, as was

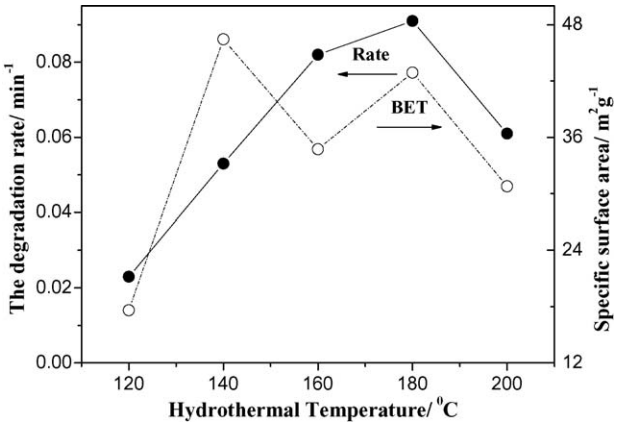

Fig. 10. Changes in the photodegradation rate and specific surface area of the as-prepared samples with the hydrothermal temperature.

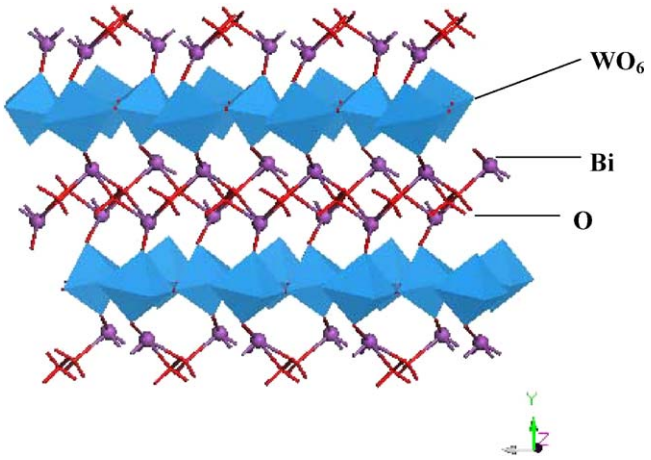

Fig. 11. Schematic structure of Bi_2WO_6 photocatalyst.

confirmed by its TEM (Fig. 1), XRD (Fig. 3) and LRS (Fig. 4). This indicates that the crystallinity is the more important factor that affects photocatalytic activity of the as-prepared sample. It is well known that lattice defects may act as recombination centers for the photoinduced electrons and holes, thus significantly reducing the net photocatalytic activity [33,34]. The decrease in the photocatalytic activity when the sample is prepared at the lower temperature may therefore be understood in such a way, namely, that the abundant lattice defects acting as inactivation centers are increased due to its poor crystallinity, which could be observed from the XRD (Fig. 3) and LRS (Fig. 4) results. Quantitative results give the atomic ratio of 1.95:1 for Bi/W when the sample was prepared at 180 °C (Table 1). It was close to the ideal value of 2 considering the instrumental error. As for the sample prepared at 120 °C, the ratio of Bi/W is only 1.87:1. The defects induced by non-stoichiometry can also be an additional reason for drastically decreased photocatalytic activity. On the other hand, the sample prepared at 200 °C revealed the lower activities for the RhB photodegradation, which could be mainly attributed to a poorer crystalline phase, which is consistent with the XRD and TEM results.

4.2. Crystal structure and morphology

The crystal structure of a photocatalyst also heavily affects its photocatalytic activity. The schematic structure of Bi_2WO_6 is presented in Fig. 11. The photocatalyst belong to the orthorhombic system, space group $Pca2_1$. Bi_2WO_6 crystal with a layered structure includes the corner-shared WO_6. Bi atoms layers are sandwiched between WO_6 octahedral layers. The lattices parameters of Bi_2WO_6 were refined by the least-squares method. The results of the refinement were as follows: $a = 0.5437$ nm, $b = 1.643$ nm, $c = 0.5458$ nm.

Table 1
The ratio of Bi:W in Bi_2WO_6 samples prepared at the different hydrothermal temperatures

Hydrothermal temperature (°C)	The ratio of Bi:W
120	1.87:1
140	1.88:1
160	1.94:1
180	1.95:1
200	1.95:1

The high photoactivity of Bi_2WO_6 catalyst could be attributed to the WO_6 layered structure, which is beneficial to the transfer of electrons to the surface of the photocatalyst along the layered network. It has been reported that a series of layered structure compounds show high activity for water splitting under irradiation, and this kind of structure was found to promote the generation and the separation of the charge carriers [35,36]. For example, Kudo et al. [37] found that layered metal oxide semiconductor particles evolve hydrogen more easily because the photogenerated electron–hole pairs can move effectively to the surface.

Generally, the e^-/h^+ recombination in the materials is divided into two categories: volume recombination and surface recombination. Volume recombination is a dominant process in well-crystallized bulk materials [39]. However, as for a unique sheet-shaped Bi_2WO_6, the surface e^-/h^+ recombination is mainly due to abundant surface trapping sites and insufficient driving force for e^-/h^+ pair separation. Thus, the highly photocatalytic efficiency of Bi_2WO_6 nanosheet is expected by accelerating the interfacial charge carrier transfer processes, increasing the amount of adsorbed RhB, selecting suitable conditions of reaction kinetics such as mass-transfer rate of RhB, and modifying the catalyzer surface, such as deposition of metals. In summary, the e^-/h^+ recombination occurred on the semiconductor surface is easier to control [39]. There have a large space to enhance the photochemical activity of the catalyst.

4.3. Bind gap and structure

In oxide semiconductors, CB levels of small band gap semiconductors are usually low because deep VB are formed by O 2p. This is a major problem for developing visible-light-driven photocatalysts. To find a breakthrough, it is indispensable to control VB with orbitals of some elements instead of O 2p. It has been found that bismuth is a potential candidate

for such a VB-control element [37]. Bi_2WO_6 could absorb visible-light because Bi 6s orbitals are attributed to the VB on the basis of DFT calculations. Furthermore, the hybridization of Bi 6s and O 2p levels makes the VB largely dispersed, which favors the mobility of the photogenerated holes in the VB and is beneficial to the oxidation reaction [25]. Therefore, Bi_2WO_6 is very active for the RhB degradation under visible-light irradiation ($\lambda > 420$ nm).

It is difficult to determine the flat band potentials of Bi_2WO_6 by electrochemical measurements because its sintered electrodes are insulated. Instead, Eq. (2) reported by Scaife [38] for the oxides not containing partly filled *d*-levels can be applied for the approximate determination of the flat band potential

$$V_{fb}(\mathrm{NHE}) = 2.94 - E_g \quad (2)$$

where V_{fb} and E_g represent a flat band potential and a band gap, respectively. The band structures of Bi_2WO_6 are roughly described, as is shown in Fig. 12. On the base of this hypothesis, O_2 evolution on Bi_2WO_6 catalysts is possible because the VB potential level (+2.94 eV) is more positive than that of oxygen evolution (+1.23 eV). However, it seems impossible for hydrogen evolution due to the more positive CB potential level (+0.24 eV) compared to that of hydrogen evolution (0 eV). Tang et al. [26] have demonstrated photocatalytic O_2 evolution by Bi_2WO_6 catalyst from $AgNO_3$ solution. But they kept silence about H_2 evolution by Bi_2WO_6 catalyst from H_2O.

4.4. Photocatalytic mechanisms

Photodegradation of chemicals by the semiconductor have been studied previously [1,2]. When a photon is absorbed by the semiconductor, an e^-/h^+ pair is generated. The e^- and h^+ could migrate to the surface to react with the adsorbed reactants in the desired process, or then could undergo a non-desired recombination. A rate increase in the former process or a rate decrease in the latter would lead to greater photocatalytic efficiency [39]. Bi_2WO_6 catalyst could efficiently degrade RhB, $CHCl_3$ and CH_3CHO under visible irradiation [26]. Therefore, the photocatalyst with a strong oxidizing potential could be postulated.

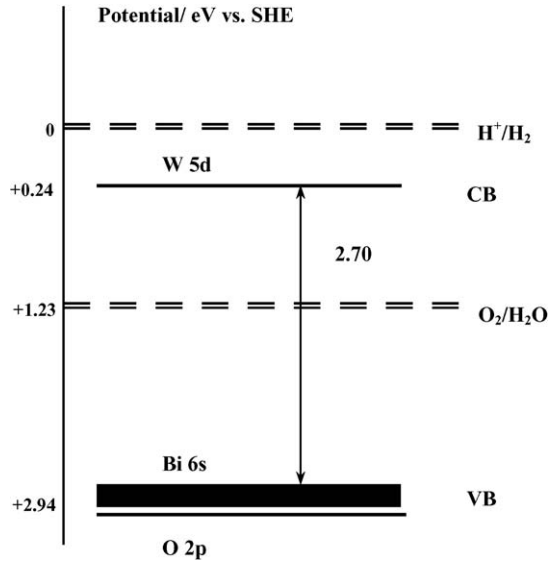

Fig. 12. Band structures of Bi_2WO_6 photocatalyst. The VB and CB levels of Bi_2WO_6 are roughly estimated by Eq. (2).

Meanwhile, Bi_2WO_6 catalyst also showed the activity when the light wavelength was much longer than 490 nm, where it absorb poorly the light radiation. It is well known that RhB can absorb visible-light in the range 400–600 nm, which is attributed to the ground state and the excited state of the dye. RhB is the main material absorbing light irradiation when $\lambda > 490$ nm. So, it is postulated that the RhB photodegradation is attributed to the photosensitized process [1,3,40]. When $\lambda > 490$ nm, RhB is only the light absorbing species. From the dye-excited state, an electron is injected into the CB of Bi_2WO_6 where it is captured by the surface adsorbed O_2 to produce $O_2^{-\bullet}$, and the dye cation radicals are decomposed subsequently via attack by oxygen active species. Compared to the photocatalytic process, the efficiency in the photosensitized process is very low. Furthermore, it could be speculated that no further photodegradation of dye pollutants occurs once the dye is bleached; the complete mineralization of the dye could not be achieved [40].

It was well reported that the RhB photodegradation occurs via two competitive processes: *N*-demethylation and the destruction of the conjugated structure [40]. In the present work, the RhB decomposition under UV irradiation mainly occurs via the destruction of the conjugated structure. Therefore, the absorbance spectra revealed no new absorption features, indicating that no new intermediates or products formed during this photochemical process. The yield of NH_4^+ was lower compared to that in the case of visible irradiation, although the higher mineralized degree was achieved. We concluded that the nitrogen-containing fractions still exist in the suspension even at the latter stage, when the RhB photodegradation is via the destruction of the conjugated structure.

In the case of visible light irradiation, loss of RhB was mainly attributed to the *N*-demethylation process. The absorbance spectra of the suspension shifted gradually toward the blue region, and ultimately, a new absorbance band at 503 nm^{-1} appeared, suggesting the fully de-ethylated RhB molecule formed [39]. When RhB was transformed via the *N*-demethylation, nitrogen atoms could directly be liberated into the solution in the form of NH_4^+, result in the higher yield of NH_4^+ under visible-light irradiation.

5. Conclusions

Nanosized Bi_2WO_6 catalyst was prepared via the hydrothermal process. The as-prepared samples exhibited relatively high surface areas. The qualities of the resulting products were very sensitive to the hydrothermal temperature. The combined characterizations of TEM, XRD and LRS illuminated that the sample prepared at 180 °C exhibited the high crystallinity. The DFT calculations suggested that the visible-light response of Bi_2WO_6 catalyst was due to the transition form the VB formed

by the hybrid orbitals of Bi 6s and O 2p to the CB of W 5d. Dependence of the photocatalytic activities on the hydrothermal temperature was then examined under visible-light irradiation ($\lambda > 420$ nm). The most samples exhibited the higher photoactivities as compared to $TiO_{2-x}N_x$. The sample prepared at 180 °C exhibited the highest photochemical activity. The further experiments revealed that Bi_2WO_6 photocatalyst was active for the RhB decomposition in the wide wavelength range, including both UV and visible-light, but a difference in the photodegradation mechanisms of RhB could be postulated.

Our work suggests that the idea of using Bi_2WO_6 could be a plausible strategy to develop an efficient photocatalyst for the destruction of the pollutants, especially by using visible-light. The hydrothermal technique presented here seems an economical and fast way for the preparation of such material.

Acknowledgments

This work was partly supported by Chinese National Science Foundation (20433010, 20571047) and Trans-Century Training Program Foundation for the Talents by the Ministry of Education, PR China, and China Postdoctoral Science Foundation (2005037050) for financial support.

Appendix A. Supplementary data

Supplementary data associated with this article can be found, in the online version, at doi:10.1016/j.apcatb.2006.02.022.

References

[1] M.R. Hoffmann, S.T. Martin, W. Choi, Chem. Rev. 95 (1995) 69.
[2] M.A. Fox, M.T. Dulay, Chem. Rev. 93 (1993) 341.
[3] C.C. Wong, W. Chu, Environ. Sci. Technol. 37 (2003) 2310.
[4] W. Ho, J. Yu, J. Lin, P. Li, Langmuir 20 (2004) 5865.
[5] W. Choi, S. Kim, Environ. Sci. Technol. 36 (2002) 2019.
[6] H. Kominami, S. Murakami, J. Kato, Y. Kera, B. Ohtani, J. Phys. Chem. B 106 (2002) 10501.
[7] J. Yu, L. Zhang, Z. Zheng, J. Zhao, Chem. Mater. 15 (2003) 2280.
[8] A. Maurizio, A. Vincenzo, D.P. Agatino, J. Phys. Chem. B 108 (2004) 3303.
[9] M. Andersson, L. Osterlund, S. Ljungstrom, A. Palmqvist, J. Phys. Chem. B 106 (2002) 10674.
[10] R. Asahi, T. Morikawa, T. Ohwaki, K. Aoki, Y. Taga, Science 293 (2001) 269.
[11] I. Hiroshi, W. Yuka, H. Kazuhito, J. Phys. Chem. B 107 (2003) 5483.
[12] M. Mrowetz, W. Balcerski, A. Colussi, M. Hoffmann, J. Phys. Chem. B 108 (2004) 17269.
[13] P. Reddy, B. Sun, G. Smirniotis, J. Phys. Chem. B 108 (2004) 17198.
[14] X. Fu, A. Clark, Q. Yang, A. Anderson, Environ. Sci. Technol. 30 (1996) 647.
[15] Z. Zou, J. Ye, K. Sayama, H. Arakawa, Nature 414 (2001) 625.
[16] K. Domen, A. Kudo, T. Onishi, J. Catal. 10 (1986) 217.
[17] H. Kato, A. Kudo, Catal. Lett. 295 (1998) 487.
[18] K. Sayama, H. Arakawa, J. Phys. Chem. 97 (1993) 531.
[19] A. Kudo, K. Sayama, A. Tanaka, K. Asakura, K. Domen, K. Maruya, T. Onishi, J. Catal. 120 (1989) 337.
[20] K. Sayama, H. Arakawa, J. Photochem. Photobiol. A: Chem. 77 (1994) 243.
[21] Y. Inoue, T. Kubokawa, K. Stao, J. Chem. Soc., Chem. Commun. (1990) 1298.
[22] J. Tang, Z. Zou, J. Ye, Angew. Chem. Int. Ed. 43 (2004) 4463.
[23] V. Nagirnyi, M. Kirm, A. Kotlov, A. Lushchik, L. Jonsson, J. Luminesci. 102 (2003) 597.
[24] Y. Shi, S. Feng, C. Cao, Mater. Lett. 44 (2000) 215.
[25] A. Kudo, S. Hijii, Chem. Lett. (1999) 1103.
[26] J. Tang, Z. Zou, J. Ye, Catal. Lett. 92 (2004) 53.
[27] (a) C. Zhang, Y. Zhu, Chem. Mater. 17 (2005) 3537;
(b) H. Fu, C. Pan, W. Yao, Y. Zhu, J. Phys. Chem. B 109 (2005) 22432.
[28] M. Crane, R. Forst, P. Williams, T. Kloprogge, J. Raman Spectrosc. 33 (2002) 62.
[29] W. Kohn, L.J. Sham, Phys. Rev. A 140 (1965) 1133.
[30] J.P. Perdew, Y. Wang, Phys. Rev. B 45 (1992) 13244.
[31] A. Kuda, H. Kato, S. Nakagawa, J. Phys. Chem. B 104 (2000) 517.
[32] Z. Zou, J. Ye, H. Arakawa, J. Phys. Chem. B 106 (2002) 13098.
[33] M. Yoshino, M. Kakihana, Chem. Mater. 14 (2002) 3369.
[34] Z. Zou, J. Ye, H. Arakawa, J. Phys. Chem. B 106 (2002) 517.
[35] E. Yasuo, S. Takayoshi, H. Masaru, W. Mamoru, Chem. Mater. 14 (2002) 4309.
[36] Z. Lei, W. You, M. Liu, G. Zhou, T. Takata, M. Hara, K. Domen, C. Li, Chem. Commun. (2003) 2142.
[37] A. Kudo, K. Omori, H. Kato, J. Am. Chem. Soc. 121 (1999) 11459.
[38] D.E. Scaife, Sol. Energy 25 (1980) 41.
[39] N. Bao, X. Feng, Z. Yang, L. Shen, X. Lu, Environ. Sci. Technol. 38 (2004) 2729.
[40] C. Chen, X. Li, W. Ma, J. Zhao, J. Phys. Chem. B 106 (2002) 318.